HYDROGEN, FUEL CELL & ENERGY STORAGE

# Thermo-Economic Analysis of Triple Production System, Combination with Solid Oxide Fuel Cell and Absorption Chiller

**Sonia Hosseini**[a] | **Jamasb Pirkandi**[b] | **Zahra Poolaei Moziraji**[c,*]

[a] Department of Mechanical Engineering, Damavand Branch, Islamic Azad University, Tehran, Iran
[b] Malek Ashtar University of technology, Tehran, Iran
[b] Department of Mechanical Engineering, North Tehran Branch, Islamic Azad University, Tehran, Iran
[*] Corresponding author, Email: z.poolaei@iau-tnb.ac.ir

**Article Information**

**Article Type**
Research Article

**Article History**
Received: *10 Oct 2024*
Revised: *15 Nov 2024*
Accepted: *20 Dec 2024*
Published Online: *04 Jan 2025*

**Keywords**

Gas turbine
Solid oxide fuel cell
Absorption chiller
Exergy
Economic analysis

**Abstract**

This article introduces and analyzes the thermodynamic and economic performance of two triple hybrid systems that generate power, thermal and refrigeration energy. The primary drive is a hybrid cycle consisting of a gas turbine and solid oxide fuel cell, supplemented by single-effect and double-effect absorption chillers as the secondary drive. Given the significance of the fuel cells in this system, detailed thermodynamic and thermal and electrochemical analyses have been conducted to ensure accurate calculations. The study examines that the impact of the compressor pressure ratio and air-to-fuel ratio on energy and exergy efficiency, exergy destruction and exergy loss rates, system costs and heating and cooling production. Results indicate that increasing the compressor pressure ratio enhances electrical and exergy efficiency system while reducing exergy destruction rates and electricity costs. Additionally, switching from a single-effect to a double-effect absorption chiller reduces exergy destruction by 5.4% but increases electricity production costs by 28%.

**Cite this article:** Hosseini, S., Pirkandi, J., Poolaei Moziraji, Z. (2025). Thermo-Economic Analysis of Triple Production System, Combination with Solid Oxide Fuel Cell and Absorption Chiller. DOI: 10.22104/hfe.2024.7021.1308

 Publisher: Iranian Research Organization for Science and Technology (IROST)
DOI: 10.22104/hfe.2024.7021.1308

# 1 Introduction

As societies evolve and energy consumption rises amidst dwindling natural resources, it is crucial to use available resources efficiently to minimize waste. Proposed solutions must be economically and environmentally justifiable. To address these challenges, alternative approaches have been explored, emphasizing reduced energy consumption and enhanced performance. One notable trend in energy management is the use of thermodynamic cycles in power plants and generation industries, as well as in heating and cooling discussions. [1]. Simultaneous production refers to generating two or more useful forms of energy from one or two energy sources. Typically, this involves converting fuel into thermal (heating and cooling) and mechanical (power generation) energies. Recent studies have extensively examined synchronous production cycles due to their numerous advantages and applications. Such systems are utilized in food industries, hotels, shopping centers, airports, hospitals, and homes [1].

The efficient use of energy resources in simultaneous production systems is crucial. These resources should be chosen to minimize environmental impact. Researchers are particularly focused on the production of cooling in these systems, making it a key area of study. Primary drives that serve as the main energy suppliers include gas turbines, steam turbines, fuel cells, micro-turbines, and internal combustion engines. Fuel cell systems, regarded as the fourth generation of power plants, generate electricity through a distinct electrochemical process, similar to batteries. They offer a clean, efficient, and quiet means of electricity generation. Since fuel cells consume fuel in an electrochemical reaction rather than through combustion, they do not contribute to air pollution [1].

Research on hybrid systems began in 1970, but investigations reveal that there has been limited study on triple hybrid systems involving fuel cells, gas turbines, and absorption chillers. Chen et al. [2] researched and optimized a multi-home production system that integrates a molten carbonate fuel cell and an absorption chiller to generate heat, cooling, and power. Yang et al. [3] developed and thermodynamically analyzed a system that simultaneously produces electricity, heat, and cooling using a solid oxide fuel cell, gas turbine, and liquid hydrogen. Ho et al. [4] analyzed a system that simultaneously produces electricity, heat, and cooling from both thermodynamic and economic perspectives. The system comprises a gas turbine, steam turbine, and methanol reforming.

Liu et al. [5] examined the thermodynamic performance and exergy of a simultaneous production system for electricity, heat, and cooling using solid oxide fuel cells, the Brayton cycle, and the Rankine cycle. Marefati et al. [6] analyzed and investigated a triple simultaneous production system based on solid oxide fuel cell, solar cells, Stirling engine and steam turbine. Moghadam et al. [7] evaluated the thermodynamic performance and exergy of a new system that simultaneously produces electricity, heat, and cooling using a gas turbine, Kalina cycle, and absorption chiller. In a research, Ping Pang et al [8] analyzed the energy and exergy of a new system consisting of a solid oxide fuel cell, a solar collector and a steam turbine for the simultaneous production of electricity, heat and cooling.

In an economic study, Da Silva and Matelli [9] analyzed the cost of power generation in a combined system of molten carbonate fuel cells and steam turbines. Hosseini et al. [10] reviewed and assessed the economic performance of a new hybrid system that includes a molten carbonate fuel cell, a methanol synthesis system, and a power generation cycle. Zeng and colleagues [11] explored the thermodynamics of a triple system combining heat, power, and cooling using a solid oxide fuel cell, a Rankine cycle, and a double-effect absorption chiller. Zehang and his team [12] examined the thermos-economics of a combined heat, power, and cooling system utilizing a solid oxide fuel cell and a $CO_2$ supercritical cycle. Behzadi and his colleagues [13] analyzed the thermodynamics of a hybrid system that includes a solid oxide fuel cell, gas turbine, and double-effect absorption chiller. Zheng et al. [14] conducted a thermodynamic performance analysis of a triple system for heat, cooling, and power generation that integrates a solid oxide fuel cell, electrolyzer, and energy and heat storage.

Wang et al. [15] performed thermodynamic, exergy, and economic analyses of two configurations combining a solid oxide fuel cell and gas micro turbine with a solar-powered methane reforming system for heat, cooling, and power production. Zheng et al. [16] analyzed a new system combining an electrolyzer and solid oxide fuel cell for power, heating, cooling, and heat storage, utilizing solar energy. This system features a polymer membrane electrolyzer, solid oxide fuel cell, heat storage, and photovoltaic components. Yang et al [17], performed thermodynamic and exergy analysis of a new hybrid system of polymer membrane electrolyzer with solid oxide fuel cell based on biomass fuel to produce power, heat and cooling. This system includes polymer membrane electrolyzer, biomass gasifier, solid oxide fuel cell and single effect absorption chiller.

Ghorbani et al [18], performed a parametric study and optimization of a triple cooling, heating and power production system based on geothermal energy. The cogeneration system consists of three subsystems,

namely the Kalina cycle, the ejector refrigeration cycle and the organic Rankine cycle.

Zhang et al [19], conducted a thermodynamic, exergy and economic study of the performance of a new hybrid three generation system with solid oxide fuel cell and high temperature proton membrane electrolyzer based on biomass fuel. This system includes solid oxide fuel cell, absorption chiller, Carnot cycle, proton membrane electrolyzer and biomass gasification process. Jia and Paiol [20], analyzed and evaluated a combined system of Stirling engine, internal combustion engine and absorption chiller to produce heat, cooling and power from economic and thermodynamic point of view. Huang et al [21], performed thermodynamic, economic and environmental analysis and optimization of a combined power, heat and cooling system based on solid oxide fuel cell and gas turbine. This new system includes solid oxide fuel cell, gas turbine, Rankine cycle, organic Rankine cycle, ejector refrigeration system and heat exchanger. Huang et al [22], performed a thermodynamic analysis of a triple production system of heat, cooling and power with hydrogen production process with methane reforming based on solar energy. This system includes several sub-systems including hydrogen production sub-system, gas turbine and fuel cell combination, double-effect thermal absorption chiller with heat pump and home spa production sub-system. Wang et al [23], analyzed and investigated a new triple production system of refrigeration, heating and power based on biomass combustion, $CO_2$ supercritical cycle, single effect absorption chiller and desalination. The presented system consists of a supercritical $CO_2$ cycle, a single-effect absorption chiller, a heat supply unit and a multi-effect desalination subsystem.

This article presents two configurations of hybrid simultaneous production systems primarily powered by a gas turbine and solid oxide fuel cell (SOFC+GT) hybrid cycle, supplemented by single-effect and double-effect absorption chillers. The systems and their peripheral equipment will be modeled and analyzed from thermodynamic, exegetical, and economic perspectives. Unlike most studies, this research examines fuel cells separately in three parts: optimization, electrochemical processes, and thermal calculations. A parametric study of the hybrid systems will assess the impact of compressor pressure ratio, air-to-fuel ratio, and generator output temperature on energy efficiency, exergy destruction and waste, system irreversibility, and cost. The system has been evaluated.

## 2 Modeling of Proposed Systems

The proposed hybrid systems are illustrated in Figures 2 and 3, representing the first and second systems, respectively. The first system features a combined cycle of a gas turbine, fuel cell, and single-effect absorption chiller. The second system utilizes a combined cycle of a gas turbine, fuel cell, and double-effect absorption chiller. The natural gas used consists of 97% methane, 1.5% carbon dioxide, and 1.5% nitrogen, while the solid oxide fuel cell serves as the primary driver in both systems. The air entering the cycle comprises 21% oxygen and 79% nitrogen.

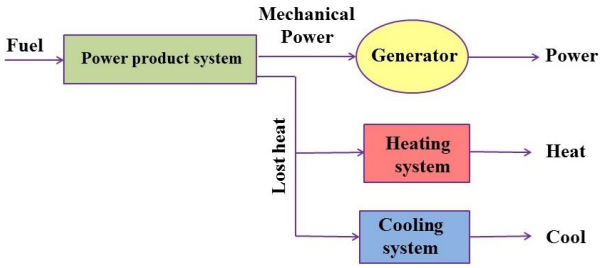


**Fig. 1. Production cycle of the triple system.**

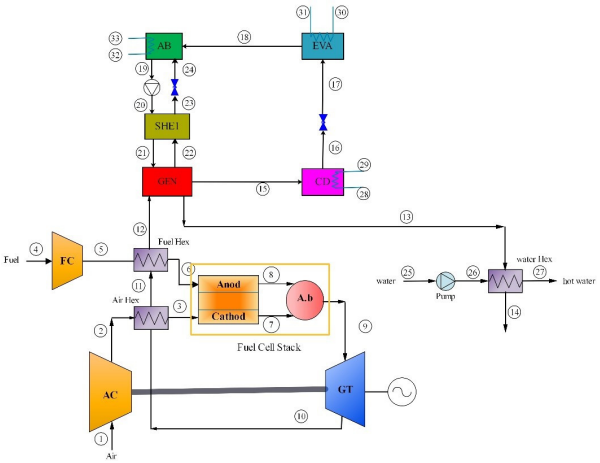


**Fig. 2. The proposed hybrid system features a single-effect absorption chiller (the first proposed system).**

**Table 1. Summary of the conducted research.**

| No. | Researcher | Year | Hybrid system | Type analysis |
|---|---|---|---|---|
| 1 | Chen et al. | 2018 | Molten carbon fuel cell combined with an absorption chiller | Thermodynamic, economic and environmental analysis |
| 2 | Yang et al. | 2020 | Including solid oxide fuel cell, gas turbine and liquid hydrogen | Thermodynamic analysis |
| 3 | Ho et al. | 2018 | Gas turbine, steam turbine, and methanol reforming | Thermodynamic and economic analysis |
| 4 | Liu et al. | 2019 | solid oxide fuel cells, Brayton and Rankine cycles, carbon dioxide, and liquid hydrogen fuel | Thermodynamic and exergy analysis |
| 5 | Marefati et al. | 2019 | Solid oxide fuel cells, solar cells, Stirling engines, and steam turbines. | Thermodynamic analysis |
| 6 | Moghadam et al. | 2021 | Gas turbine, Kalina cycle, and absorption chiller. | Thermodynamic and exergy analysis |
| 7 | Ping Pang et al. | 2020 | Including solid oxide fuel cell, solar collector and steam turbine | Energy and exergy analysis |
| 8 | Dasilvar and Mutli | 2019 | Including molten carbon fuel cell and steam turbine | Exergeoeconomics review |
| 9 | Hosseini et al. | 2019 | including molten carbonate fuel cell, methanol synthesis system | Economic Analysis |
| 10 | Zeng et al. | 2021 | including solid oxide fuel cell, Rankine cycle and double effect absorption chiller | Thermodynamic analysis |
| 11 | Zhang et al. | 2021 | Including solid oxide fuel cell and $CO_2$ supercritical cycle | Thermoeconomic analysis |
| 12 | Behzadi et al. | 2019 | Including solid oxide fuel cell, a gas turbine and a double-effect absorption chiller | Thermodynamic analysis |
| 13 | Zheng et al | 2022 | Including solid oxide fuel cell, electrolyzer and energy and heat storage | Thermodynamic analysis |
| 14 | Wang et al. | 2023 | Including solid oxide fuel cell, gas micro turbine connected to methane reforming system based on solar energy | Thermodynamic, exergy and economic analysis |
| 15 | Zheng et al | 2023 | Including polymer membrane electrolyzer, solid oxide fuel cell, heat storage and photovoltaic | Thermodynamic, exergy and economic analysis |
| 16 | Yang et al | 2023 | Including polymer membrane electrolyzer, biomass gasifier, solid oxide fuel cell and single effect absorption chiller | Thermodynamic and exergy analysis |
| 17 | Ghorbani et al | 2023 | Including of three subsystems, namely the Kalina cycle, the ejector refrigeration cycle and the organic Rankine cycle | parametric study and optimization |
| 18 | Zhang et al | 2024 | Including solid oxide fuel cell, absorption chiller, Carnot cycle, proton membrane electrolyzer and biomass gasification | Thermodynamic, exergy and economic analysis |
| 19 | Jia and Paiol | 2024 | Including Stirling engine, internal combustion engine and absorption chiller | economic and thermodynamic analysis |
| 20 | Huang et al | 2024 | Including solid oxide fuel cell, gas turbine, Rankine cycle, organic Rankine cycle, ejector refrigeration system and heat exchanger | Thermodynamic, economic and environmental analysis and optimization |

Air enters the compressor at ambient pressure and temperature, condenses, and then flows into the fuel cell anode and the afterburner chamber. Simultaneously, hydrocarbon fuel is compressed and also enters these components. The reaction of hydrogen and oxygen in the fuel cell generates significant electrical

power, enhancing the hybrid system's efficiency. After passing through the microturbine, hot gases flow into three recuperators. The exhaust gases then enter the absorption chiller generator, supplying the necessary heat for its operation. Finally, a regenerator provides hot water at the end of the cycle. In this hybrid system, the fuel cell, gas turbine, absorption chiller, and regenerator collectively generate thermal energy, increasing both efficiency and power output.

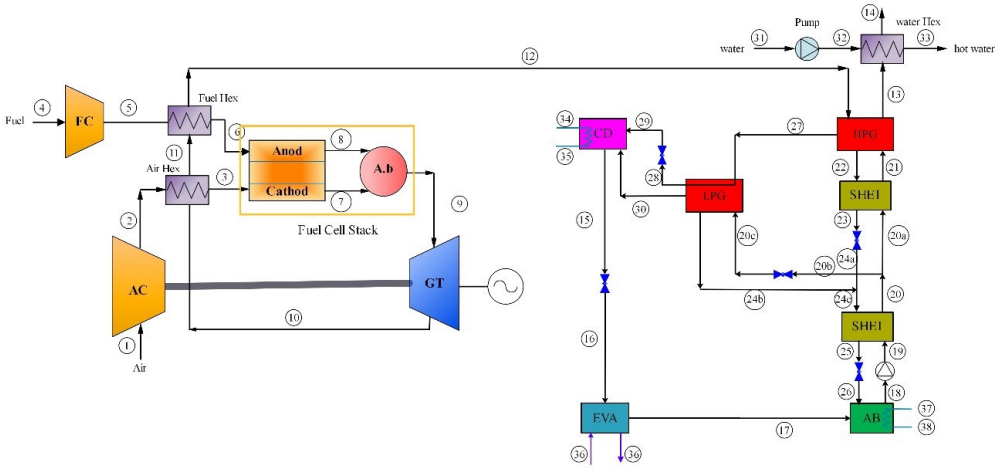


**Fig. 3. Composition of the proposed hybrid system featuring a double-effect absorption chiller (the second proposed system).**

## 3 Assumptions

The modeling and analysis of the proposed hybrid systems have considered the following assumptions:

- All aspects of the adiabatic cycle are assumed.
- Flow is stable across all components.
- The behavior of all gases used in the ideal cycle is assumed.
- Gas leakage from the system to the outside is minimal.
- The voltage across the fuel cells is assumed to be constant.
- The fuel cell is believed to convert its fuel into hydrogen through internal optimization.
- The isentropic efficiency of compressors is assumed to be 70%.
- The isentropic efficiency of the turbine is considered to be 80%.
- The efficiency of heat exchangers is assumed to be 95%.
- Ambient temperature water is used for cooling in the absorber and condenser.

## 4 Governing Equations

This section examines the performance of all system components under stable conditions. A computer program was developed using EES software to evaluate system performance by varying key parameters, including the compressor's working pressure ratio, turbine inlet gas temperature, evaporator inlet water temperature, cooling tower inlet temperature, and generator inlet temperature. The governing relations are presented in two parts: thermodynamic and economic relations.

### 4.1 Thermodynamic relationships

Thermodynamic relations are given in Table 2.

### 4.2 Absorption chiller modeling

The energy balance for each of the components of the single-effect refrigeration system, including the generator, condenser, evaporator, and observer, is according to Table 3 [24].

The system performance coefficient is defined by the following relationship:

$$\mathrm{COP} = \frac{Q_{\mathrm{ev}}}{Q_g + W_p}\,. \tag{1}$$

Exergy efficiency is calculated using the following equation:

$$\eta_{\mathrm{exergy}} = \frac{Q_{\mathrm{eva}}\left(1 - \frac{T_0}{T_b}\right)}{Q_{\mathrm{gen}}\left(1 - \frac{T_0}{T_b}\right) + W_p}\,. \tag{2}$$

**Table 2. Energy balance, Exergy balance and Exergy destruction relations [25, 26] (to be continued).**

| Exergy balance | Energy balance | Components |
|---|---|---|
| Air Compressor | $\frac{T_2}{T_1} = \left(\frac{P_2}{P_1}\right)^{\frac{k_a-1}{k_a \eta_{p,\mathrm{ca}}}}$<br>$\eta_{\mathrm{is},c} = \frac{w_{c,s}}{w_{c,a}} = \frac{\bar{h}_{2s} - \bar{h}_1}{\bar{h}_2 - \bar{h}_1}$<br>$W_C = n_{\mathrm{ca}} w_{c,a}$ | $S_{\mathrm{gen,ca}} = n_{\mathrm{ca}}(\bar{s}_2 - \bar{s}_1)$<br>$E_{D,\mathrm{ca}} = W_{\mathrm{ca}} - n_{\mathrm{ca}}(e_2 - e_1)$<br>$\psi_{\mathrm{ca}} = \frac{n_{\mathrm{ca}}(e_2 - e_1)}{W_{\mathrm{ca}}}$ |
| Fuel Compressor | $\frac{T_5}{T_4} = \left(\frac{P_5}{P_4}\right)^{\frac{k_a-1}{k_a \eta_{p,\mathrm{fa}}}}$<br>$\eta_{\mathrm{is,cf}} = \frac{w_{c,s}}{w_{c,f}} = \frac{\bar{h}_{5s} - \bar{h}_4}{\bar{h}_5 - \bar{h}_4}$<br>$W_C = n_{\mathrm{cf}} w_{c,f}$ | $S_{\mathrm{gen,cf}} = n_{\mathrm{cf}}(\bar{s}_5 - \bar{s}_4)$<br>$E_{D,\mathrm{cf}} = W_{\mathrm{cf}} - n_{\mathrm{cf}}(e_5 - e_4)$<br>$\psi_{\mathrm{cf}} = \frac{n_{\mathrm{cf}}(e_5 - e_4)}{W_{\mathrm{cf}}}$ |
| Gas Turbine | $\frac{T_9}{T_{10,s}} = \left(\frac{P_9}{P_{10}}\right)^{\frac{k_g-1}{k_g}}$<br>$\eta_{\mathrm{is,gt}} = \frac{w_{\mathrm{gt},a}}{w_{\mathrm{gt},s}} = \frac{\bar{h}_9 - \bar{h}_{10}}{\bar{h}_9 - \bar{h}_{10,s}}$<br>$W_{\mathrm{gt}} = n_9(\bar{h}_9 - \bar{h}_{10})$ | $S_{\mathrm{gen,gt}} = n_{\mathrm{gt}}(\bar{s}_9 - \bar{s}_{10})$<br>$E_{D,\mathrm{gt}} = n_{\mathrm{gt}}(e_9 - e_{10}) - W_{\mathrm{gt}}$<br>$\psi_{\mathrm{gt}} = \frac{W_{\mathrm{gt}}}{n_{\mathrm{gt}}(e_9 - e_{10})}$ |
| Heat exchanger I | $\epsilon_{\mathrm{reg},1} = \frac{T_3 - T_2}{T_{10} - T_2}$ | $S_{\mathrm{gen,reg},1} = n_2(\bar{s}_3 - \bar{s}_2) - n_{10}(\bar{s}_{10} - \bar{s}_{11})$<br>$E_{D,\mathrm{reg},1} = n_{10}(e_{10} - e_{11}) - n_2(e_3 - e_2)$<br>$\psi_{\mathrm{reg},1} = \frac{n_2(e_3 - e_2)}{n_{10}(e_{10} - e_{11})}$ |
| Heat exchanger II | $\epsilon_{\mathrm{reg},2} = \frac{T_6 - T_5}{T_{11} - T_5}$ | $S_{\mathrm{gen,reg},2} = n_5(\bar{s}_6 - \bar{s}_5) - n_{10}(\bar{s}_{11} - \bar{s}_{12})$<br>$E_{D,\mathrm{reg},2} = n_{10}(e_{11} - e_{12}) - n_5(e_6 - e_5)$<br>$\psi_{\mathrm{reg},2} = \frac{n_5(e_6 - e_5)}{n_{10}(e_{11} - e_{12})}$ |
| Heat exchanger III | $Q_{\mathrm{reg},3} = \epsilon_{\mathrm{reg},3} n_{12}(\bar{h}_{12} - \bar{h}_{13})$<br>$Q_{\mathrm{reg},3} = n_{\mathrm{water}} \bar{C}_P (T_{12} - T_{13})$ | $S_{\mathrm{gen,reg},3} = n_{26}(\bar{s}_{27} - \bar{s}_{26}) - n_{10}(\bar{s}_{13} - \bar{s}_{14})$<br>$E_{D,\mathrm{reg},3} = n_{10}(e_{13} - e_{14}) - n_{26}(e_{27} - e_{26})$<br>$\psi_{\mathrm{reg},3} = \frac{n_{26}(e_{27} - e_{26})}{n_{10}(e_{13} - e_{14})}$ |
| Water Pump | $\eta_{\mathrm{is},P,W} = \frac{w_{\mathrm{is}}}{w_{\mathrm{act}}} = \frac{v_{25}(P_{26} - P_{25})}{h_{26} - h_{25}}$<br>$\dot{W}_{P,W} = \dot{m}_{25}(h_{26} - h_{25})$ | $E_{D,W} = W_{P,W} + E_{25} - E_{26}$<br>$\psi_{P,W} = \frac{E_{26} - E_{25}}{W_{P,W}}$ |
| SOFC | $E = E^0 + \frac{R_u T}{n_e F} \ln\left(\frac{p_{\mathrm{O_2}} p_{\mathrm{O_2}}^{1/2}}{p_{\mathrm{H_2O}}}\right)$<br>$V_{\mathrm{cell}} = E - (V_{\mathrm{act}} + V_{\mathrm{ohm}} + V_{\mathrm{con}}) = E - \Delta V_{\mathrm{loss}}$<br>$I_{\mathrm{tot}} = 2Fz$<br>$(\dot{W}_{\mathrm{DC}})_{\mathrm{sofc}} = V_{\mathrm{cell}} I_{\mathrm{tot}}$<br>$(\dot{W}_{\mathrm{AC}})_{\mathrm{sofc}} = (\dot{W}_{\mathrm{DC}})_{\mathrm{sofc}} \eta_{\mathrm{inv,sofc}}$<br>$\dot{Q}_{\mathrm{elec}} = zT\Delta S - I\Delta V_{\mathrm{loss}}$<br>$\dot{Q}_{\mathrm{net}} = \dot{Q} + \dot{Q}_{\mathrm{surr}}$<br>$Q = \Delta h_{\mathrm{ca,in}} + \Delta h_{\mathrm{ca,out}} + \Delta h_{\mathrm{an,in}} + \Delta h_{\mathrm{an,out}}$<br>$\dot{Q}_{\mathrm{error}} = \left\lvert \frac{\dot{Q}'' - \dot{Q}'}{\dot{Q}''} \right\rvert < 0.01$<br>$\dot{n}_3\bar{h}_3 + \dot{n}_4\bar{h}_4 = \dot{Q}_{\mathrm{error}} + \dot{W}_{\mathrm{sofc}} + (\dot{n}_7\bar{h}_7 + \dot{n}_8\bar{h}_8)$ | $S_{\mathrm{gen,sofc}} = (n_7\bar{s}_7 + n_8\bar{s}_8) - (n_3\bar{s}_3 + n_6\bar{s}_6) + \frac{Q_{\mathrm{surr}}}{T_{\mathrm{surr}}}$<br>$E_{D,\mathrm{sofc}} = E_3 + E_6 - E_7 - E_8 - E_Q - W_{\mathrm{sofc}}$<br>$\psi_{\mathrm{sofc}} = \frac{W_{\mathrm{sofc}}}{E_3 + E_6 - E_7 - E_8}$ |

**Table 2. Energy balance, Exergy balance and Exergy destruction relations [25, 26].**

| Exergy balance | Energy balance | Components |
|---|---|---|
| After Burner | $CO + \frac{1}{2}O_2 \longrightarrow CO_2$<br>$H_2 + \frac{1}{2}O_2 \longrightarrow H_2O$<br>$CH_4 + 2\,O_2 \longrightarrow CO_2 + 2H_2O$<br>$n_7\bar{h}_7 + n_8\bar{h}_8 - n_9\bar{h}_9 - Q_{\text{loss,ab}} = 0$<br>$Q_{\text{loss,ab}} = n_4(1-U_f)(1-\eta_{\text{ab}}) \times \text{LHV}$ | $S_{\text{gen,ab}} = n_9\bar{s}_9 - n_7\bar{s}_7 - n_8\bar{s}_8 + \frac{Q_{\text{loss,ab}}}{T_{\text{surr}}}$<br>$E_{D,\text{ab}} = E_7 + E_8 - E_9 - E_{Q,\text{ab}}$<br>$\psi_{\text{ab}} = \frac{E_9}{E_7 + E_8}$ |

**Table 3. Energy balance, Exergy balance and Exergy destructions relations [24].**

| Exergy balance | Energy balance | Components |
|---|---|---|
| Generator | $\dot{m}_{12}h_{12} + \dot{m}_{21}h_{21} = \dot{m}_{13}h_{13} + \dot{m}_{15}h_{15} + \dot{m}_{22}h_{22}$ | $E_{D,g} = E_{12} + E_{21} - E_{13} - E_{22} - E_{15}$<br>$\psi_G = \frac{Q_g}{E_{12} + E_{21}}$ |
| SHE | $\dot{m}_{20}h_{20} + \dot{m}_{22}h_{22} = \dot{m}_{23}h_{23} + \dot{m}_{21}h_{21}$ | $E_{D,\text{SHE}} = E_{22} + E_{20} - E_{23} - E_{21}$<br>$\psi_{\text{SHE}} = \frac{E_{20} - E_{21}}{E_{22} - E_{23}}$ |
| ARC Pump | $\eta_{\text{is},P,\text{ARC}} = \frac{W_{\text{is}}}{W_{\text{act}}} = \frac{v_{19}(P_{20} - P_{19})}{h_{20} - h_{19}}$<br>$\dot{W}_{P,\text{ARC}} = \dot{m}_{20}(h_{20} - h_{19})$ | $E_{D,\text{ARC},P} = W_{P,\text{ARC}} + E_{19} - E_{20}$<br>$\psi_{P,\text{ARC}} = \frac{E_{20} - E_{19}}{W_{P,\text{ARC}}}$ |
| Absorber | $\dot{m}_{19}h_{19} + \dot{m}_{13}h_{13} + \dot{m}_{53}h_{53} = \dot{m}_{54}h_{54} + \dot{m}_{14}h_{14}$ | $E_{D,\text{ab}} = E_{18} + E_{24} + E_{32} - E_{19} - E_{33}$<br>$\psi_{\text{ab}} = \frac{E_{19}}{E_{18} + E_{24}}$ |
| Expansion valve | $h_{11} = h_{12}$ | $E_{D,V} = E_{23} - E_{24}$<br>$\psi_V = \frac{E_{24}}{E_{23}}$ |
| ARC Condenser | $\dot{m}_{15}h_{15} + \dot{m}_{28}h_{28} = \dot{m}_{16}h_{16} + \dot{m}_{29}h_{29}$ | $E_{D,\text{cond}} = E_{28} + E_{15} - E_{29} - E_{16}$<br>$\psi_{\text{cond}} = \frac{Q_{\text{cond}}}{E_{15} - E_{16}}$ |
| ARC Evaporator | $\dot{m}_{17}h_{17} + \dot{m}_{30}h_{30} = \dot{m}_{18}h_{18} + \dot{m}_{31}h_{31}$ | $E_{D,\text{eva}} = E_{30} + E_{17} + E_{31} - E_{18}$<br>$\psi_{\text{eva}} = \frac{Q_{\text{eva}}}{E_{17} - E_{18}}$ |

## 4.3 Hybrid system modeling

This section considers the entire system as a control volume to calculate overall efficiency using Equation (3). In this system, heat is supplied by the third regenerator, and cooling is provided by the absorption refrigeration evaporator.

$$\eta_{\text{tot}} = \frac{W_{\text{net}} + Q_{\text{ev}} + Q_{\text{reg},3}}{n_f\,\text{LHV}}\,, \tag{3}$$

$$W_{\text{net}} = W_{\text{sofc}} + W_{\text{gt}} - W_{\text{ac}} - W_{\text{fc}} - W_{P,\text{ab}} - W_{P,w}\,, \tag{4}$$

$$\psi_{\text{sys}} = \frac{W_{\text{net}} + E_{\text{ev}} + E_{33}}{E_1 + E_4}\,, \tag{5}$$

$$E_{D,\text{sys}} = E_1 + E_4 + E_{31} - E_{14} - E_{33} - W_{\text{net}} - E_{\text{ev}}\,. \tag{6}$$

## 4.4 Economic equations

Economic analysis is crucial for assessing engineering system performance. It involves evaluating costs associated with components, operations, maintenance, and fuel consumption. Component costs can be represented as functions of the system's thermodynamic variables. Additionally, the analysis encompasses equipment purchase costs, engineering service fees, fuel prices, and maintenance expenses, all of which are amortized annually over the system's operational period. To level the annual costs, a coefficient called the capital recovery factor is used, which is defined as follows [27]:

$$\text{CRF} = \frac{i(1+i)^n}{(1+i)^n - 1} \tag{7}$$

In the relationship above, $i$ denotes the average annual effective currency depreciation rate, while $n$ indicates

the system's economic lifespan in years [27]:

$$Z_k = Z_k^{\mathrm{CI}} + Z_k^{\mathrm{OM}} \tag{8}$$

In the above equation, the overall price rate is in dollars per hour, which includes the investment price and maintenance costs. Also, the general balance equation of the price of each component will be as follows [27]:

$$\sum C_{\mathrm{out},k} + C_{w,k} = \sum C_{\in,k} + C_{q,k} + Z_k \tag{9}$$

$$C_i = c_i \mathrm{Ex}_i \tag{10}$$

**Table 4. Cost functions of system components and auxiliary relations in exergy economic analysis [28, 29].**

| Components | Cost function | auxiliary relations |
|---|---|---|
| Air Compressor | $\left(\frac{71.1\dot{m}_1}{0.9-\eta_{\mathrm{is}}}\right)\left(\frac{P_2}{P_1}\right)\ln\left(\frac{P_2}{P_1}\right)$ | $\dot{C}_2 = \dot{C}_1 + \dot{C}_{\dot{W}_{\mathrm{ac}}} + \dot{Z}_{\mathrm{AC}}$ |
| Fuel Compressor | $\left(\frac{71.1\dot{m}_4}{0.9-\eta_{\mathrm{is}}}\right)\left(\frac{P_5}{P_4}\right)\ln\left(\frac{P_5}{P_4}\right)$ | $\dot{C}_5 = \dot{C}_4 + \dot{C}_{\dot{W}_{\mathrm{ac}}} + \dot{Z}_{\mathrm{AC}}$ |
| Heat exchanger I | $4122\left(\frac{\dot{m}_{10}(h_{10}-h_{11})\times 1000}{18\Delta T_{\mathrm{lm}}}\right)^{0.6}$ | $\dot{C}_3 + \dot{C}_{11} = \dot{C}_2 + \dot{C}_{10} + \dot{Z}_{\mathrm{reg}}$ |
| Heat exchanger II | $4122\left(\frac{m_{10}(h_{11}-h_{12})\times 1000}{18\Delta T_{\mathrm{lm}}}\right)^{0.6}$ | $\dot{C}_6 + \dot{C}_{12} = \dot{C}_5 + \dot{C}_{11} + \dot{Z}_{\mathrm{reg}}$ |
| After Burner | $\left(\frac{46.08\dot{n}_{\mathrm{AB}}}{0.995-P_9/P_8}\right)[1+\exp(0.018T_9-26.4)]$ | $\dot{C}_9 = \dot{C}_7 + \dot{C}_8 + \dot{Z}_{\mathrm{AB}}$ |
| SOFC | $A_{\mathrm{sofc}}(2.96T_{\mathrm{sofc}}-1907)$ | $\dot{C}_7 + \dot{C}_8 + \dot{C}_{\dot{W}_{\mathrm{sofc}}} = \dot{C}_3 + \dot{C}_6 + \dot{Z}_{\mathrm{AB}}$ |
| Gas Turbine | $\left(\frac{479.34\dot{m}_9}{0.92-\eta_{\mathrm{is,gt}}}\right)\ln\left(\frac{P_9}{P_{10}}\right)(1+\exp(0.036T_9-54.4))$ | $\dot{C}_7 + \dot{C}_{\dot{W}_T} = \dot{C}_6 + \dot{Z}_{\mathrm{Turb}}$ |
| Generator | $130\left(A_{\mathrm{gen}}0.093\right)^{0.78}$ | $\dot{C}_{13} + \dot{C}_{15} + \dot{C}_{22} = \dot{C}_{12} + \dot{C}_{21} + \dot{Z}_{\mathrm{HPG}}$ |
| SHE | $1.3(190+310A_{\mathrm{SHE}})$ | $\dot{C}_{23} + \dot{C}_{21} = \dot{C}_{20} + \dot{C}_{22} + \dot{Z}_{\mathrm{SHE}}$ |
| Pump chiller | $3450(\dot{W}_P)^{0.71}$ | $\dot{C}_{20} = \dot{C}_{19} + \dot{C}_{\dot{W}_{P2}} + \dot{Z}_{\mathrm{pump}}$ |
| Absorber | $130\left(A_{\mathrm{abs}}0.093\right)^{0.78}$ | $\dot{C}_{19} + \dot{C}_{33} = \dot{C}_{32} + \dot{C}_{24} + \dot{C}_{18} + \dot{Z}_{\mathrm{pump}}$ |
| Condenser | $10000 + 324(A_{\mathrm{cond}})^{0.91}$ | $\dot{C}_{16} + \dot{C}_{29} = \dot{C}_{28} + \dot{C}_{15} + \dot{Z}_{\mathrm{cond}}$ |
| Evaporator | $1.3(190+310A_{\mathrm{eva}})$ | $\dot{C}_{18} + \dot{C}_{31} = \dot{C}_{17} + \dot{C}_{30} + \dot{Z}_{\mathrm{eva}}$ |
| Pump water | $3450(\dot{W}_P)^{0.71}$ | $\dot{C}_{26} = \dot{C}_{25} + \dot{C}_{\dot{W}_{P1}} + \dot{Z}_{\mathrm{pump1}}$ |
| Heat exchanger III | $4122\left(\frac{m_{50}(h_{27}-h_{26})\times 1000}{18\Delta T_{\mathrm{lm}}}\right)^{0.6}$ | $\dot{C}_{27} + \dot{C}_{14} = \dot{C}_{26} + \dot{C}_{13} + \dot{Z}_{\mathrm{reg}}$ |

## 5 Solution Method

To analyze the problem, a computer program was developed using EES software (see Figure 4). The program starts by inputting battery parameters such as working pressure, current density, air flow rate, and fuel flow rate. Given that the battery temperature varies, an initial temperature estimate is made. This estimate allows for the simultaneous solving of optimization and electrochemical nonlinear equations, along with thermal and economic equations. The results include calculations of exhaust gas composition, temperature, voltage drop, actual voltage, current, power, efficiency, electricity production cost, installation costs, and other fuel cell characteristics.

## 6 Validation

Due to the lack of experimental and analytical results for the proposed hybrid system, this research validates the fuel cell and absorption chiller separately. First, a

program for the fuel cell and gas turbine hybrid system was developed, and its results were compared with available analytical data. Next, another program was created for single-effect and double-effect absorption chillers, comparing the results to an actual sample. Finally, these two programs were integrated into a complete system for analysis of the new hybrid system.

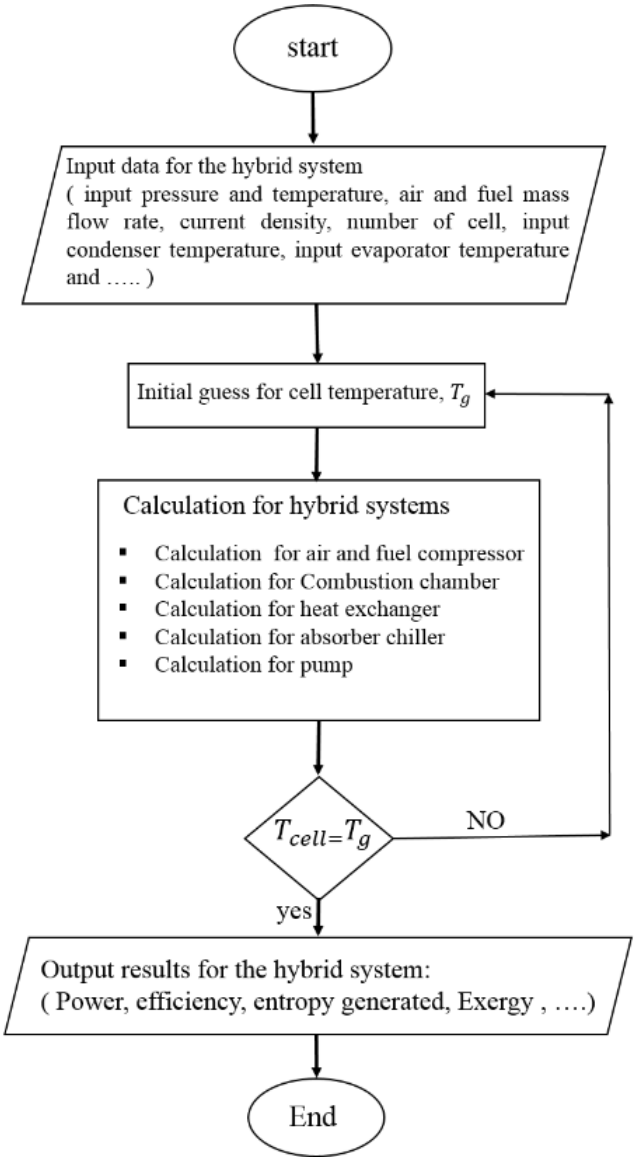


**Fig. 4. Hybrid system solution flowchart.**

### 6.1 Validation of the hybrid gas turbine and fuel cell system

To validate the prepared code, we first modeled the gas turbine and fuel cell hybrid system analyzed by Chan et al. [30], comparing our results with theirs. The close agreement confirms the accuracy of our method and code. The research employs tubular fuel cells, detailed in Table 5 [30].

**Table 5. The geometric characteristics of the fuel cell utilized in this research [30].**

| Parameters | units | The amount of assumed |
|---|---|---|
| Cell area | $m^2$ | 1036.2 |
| Cell length | m | 150 |
| Cell diameter | m | 2.2 |
| Cell number | – | 5760 |

**Table 6. Comparison of the current code results for the gas turbine and fuel cell hybrid system with the analytical results in reference [30].**

| Parameters | Ref. [30] | Present work | Error (%) |
|---|---|---|---|
| Electrical efficiency (%) | 62.2 | 60.52 | 2.7 |
| Total efficiency (%) | 83.8 | 80.62 | 3.79 |
| Heat recovery (kW) | 731 | 722.3 | 1.19 |
| Power output (kW) | 381 | 374.45 | 1.71 |
| Cell voltage (V) | 0.738 | 0.71 | 3.79 |
| Current density ($A/m^2$) | 1416 | 1416 | – |
| Cell temperature (K) | 1166 | 1166 | – |

### 6.2 Validation of the absorption chiller

This section references Gomeri's article [24] to validate the code for the chiller, which includes single-effect and double-effect series flow absorption chillers. To validate the model, inputs based on custom research were used, and the modeling results were compared with those of the custom research. As shown in Tables 7 to 9, The close alignment of these results confirms the accuracy of the current method and the developed code.

## 7 Results

This section analyzes the proposed systems from economic and thermodynamic perspectives. Key design parameters and decision variables include the compressor pressure ratio, turbine inlet temperature, evaporator outlet temperature, generator outlet temperature, and condenser outlet temperature. Assumed parameters for the proposed systems are detailed in Table 10.

**Table 7. Assumed parameters for absorption chiller [24].**

| Parameters | Amount | Parameters | Amount |
|---|---|---|---|
| Evaporator temperature ($T_{eva}$) | $4 < T_{eva} < 10$ | The water temperature outside the generator | $T_{gen} + 8$ |
| Condenser Temperature ($T_{cond}$) | $33 < T_{cond} < 39$ | Water temperature entering an absorber | $T_{cond} - 8$ |
| Absorber Temperature ($T_{abs}$) | $33 < T_{abs} < 39$ | The water temperature of an absorber | $T_{cond} - 3$ |
| Generator Temperature ($T_{gen}$) | $60 < T_{gen} < 135$ | $T_o$ (K) | 25 |
| Water temperature entering the condenser | $T_{cond} - 8$ | $P_o$ (kPa) | 101 |
| The temperature of the water exiting the condenser | $T_{cond} - 3$ | $\eta_p$ | 0.95 |
| The temperature of the water entering the evaporator | $T_{cond} + 8$ | $\epsilon$ | 0.7 |
| The water temperature exiting the evaporator | $T_{cond} + 3$ | $C_p$ (kj/kg K) | 4.18 |
| The water temperature entering the generator | $T_{gen} + 18$ | $Q_{eva}$ (kW) | 300 |

**Table 8. Comparison of the performance coefficient of a hot water lithium bromide single-effect absorption chiller in [24].**

| $T_g$(°C) | $T_{eva} = 4$ °C | | | $T_{eva} = 6$ °C | | |
|---|---|---|---|---|---|---|
| | Gomri | Present work | Error(%) | Gomri | Present work | Error (%) |
| 75 | 0.75 | 0.6404 | 2.7 | 0.75 | 0.784 | 4.5 |
| 85 | 0.76 | 0.7785 | 2.4 | 0.77 | 0.791 | 2.7 |
| 95 | 0.76 | 0.7786 | 2.4 | 0.77 | 0.787 | 2.2 |
| 105 | 0.75 | 0.7777 | 3.7 | 0.76 | 0.785 | 3.2 |

**Table 9. Comparison of the performance coefficient of a hot water lithium bromide double effect absorption chiller from [24].**

| $T_g$(°C) | $T_{eva} = 4$ °C | | | $T_{eva} = 6$ °C | | |
|---|---|---|---|---|---|---|
| | Gomri | Present work | Error (%) | Gomri | Present work | Error (%) |
| 115 | 1.18 | 1.213 | 2.8 | 1.29 | 1.333 | 3.4 |
| 125 | 1.25 | 1.281 | 2.5 | 1.35 | 1.39 | 3 |
| 135 | 1.31 | 1.341 | 2.4 | 1.36 | 1.391 | 2.3 |
| 145 | 1.32 | 1.368 | 3.7 | 1.35 | 1.392 | 3.1 |

**Table 10. Assumed parameters for the proposed system [31].**

| Parameters | Assumption |
|---|---|
| Pressure Lose | 0.04 |
| Compressor isentropic efficiency | 0.81 |
| Turbine isentropic efficiency | 0.84 |
| Chiller pressure Lose | 0.03 |
| $\eta_p$ | 0.95 |
| $\eta_{C,C}$ | 0.95 |
| Interest rate (%) | 10 |
| Escalation rate (%) | 5 |
| Plant economic life time (yr) | 20 |
| Plant working capacity rate (%) | 95 |
| Salvage value (%, percent of Initial Capital Cost) | 20 |
| Annuity factor (%) | 5 |

In the first part, the effect of the compressor pressure ratio on the system performance has been investigated. As shown in Figure 5, increasing the compressor pressure ratio causes an increases the production power and total energy of the systems. As can be seen, with the increase in the compressor pressure ratio, the production power and energy efficiency of the systems increased so that they reach their maximum value at a pressure ratio of 6 and then decrease.

As shown in Figure 6, increasing the compressor pressure ratio causes an increase in the exergy efficiency of the systems. in addition, with the increase in the pressure ratio of the compressor, the exergy destruction of the systems first decreases and increases from the pressure ratio of 6 onwards. This is because with the increase in the pressure ratio of the compressor, the production power of the system first increases and then decreases.

With the increase in the compressor pressure ratio, the production power and cooling of the second system is more than the first system, and this has increased the exergy destruction of the systems, so that this exergy destruction in the second system will be more than the first system. Also, the number of components used in the second system is more than the first system and exergy destruction will be more in them. On the other hand, with the increase in the pressure ratio of the compressor, the temperature of the exhaust gases from the turbine will increase, and this will increase the power production and exergy efficiency of the systems.

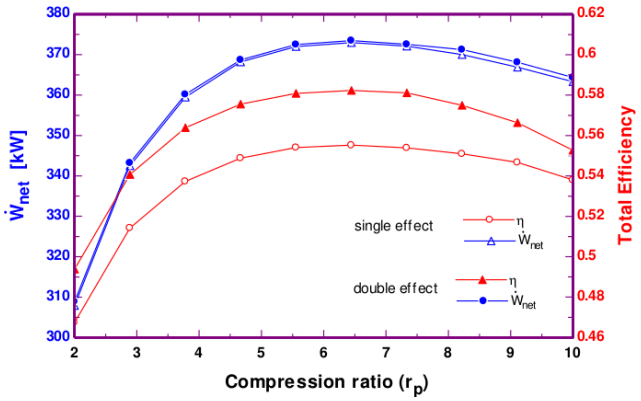


**Fig. 5. Effect of compressor pressure ratio on production power and total efficiency of the systems.**

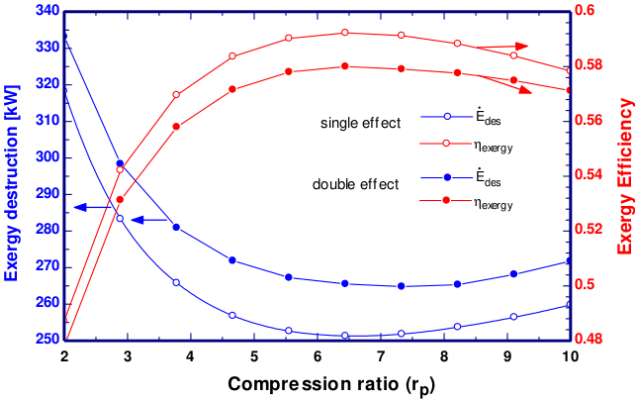


**Fig. 6. Effect of compressor pressure ratio on exergy destruction and exergy efficiency of the systems.**

Figure 7 shows the changes in the price of electricity produced by the system and its exergy efficiency according to changes in the compressor pressure ratio. As it can be seen, with the increase in the compressor pressure ratio, the price of produced electricity first decreases and then increases due to the increase in the production power of the system, so that the lowest price of produced electricity occurs at the compressor pressure ratio of 6. due to the more equipment in the second system, the price of electricity produced by the second system will be higher than the first system.

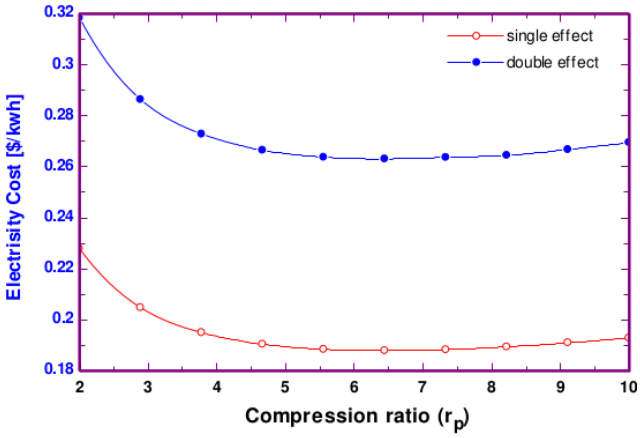


**Fig. 7. Effect of compressor pressure ratio on the price of electricity produced by the system.**

Figure 8 shows the diagram of irreversible changes and exergy loss of the system with compressor pressure changes. As can be seen, with the increase in the compressor pressure ratio, the irreversibility of the system first decreases and reaches its lowest value at the pressure ratio of 6, and then increases with the increase in the pressure ratio. On the other hand, with the increase in the pressure ratio of the compressor, the temperature of the exhaust gases from the turbine will increase, and this will increase the exergy loss of the systems. The sum of exergy destruction and exergy loss is called irreversibility, with the increase of compressor pressure ratio, exergy destruction and exergy loss increase in both systems, and this increases irreversibility. It will be in systems and this reversibility will be more in the second system than the first system.

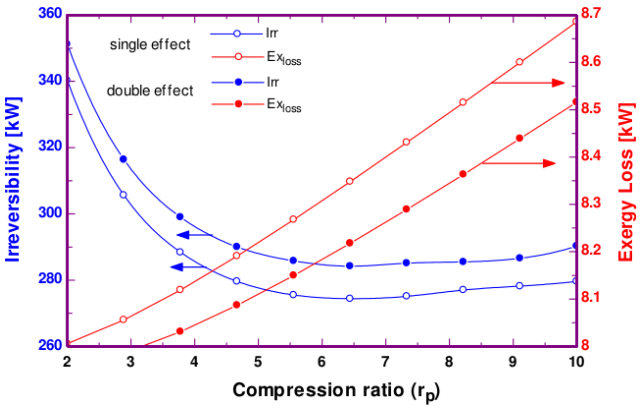


**Fig. 8. Effect of compressor pressure ratio on irreversibility and exergy loss of the systems.**

Figure 9 shows the changes in the exergy destruction of the systems with the changes in the evaporator

temperature. As the evaporator temperature rises, exergy destruction in the systems increases, leading to a decrease in cooling output. This results in reduced system efficiency and increased irreversibility, ultimately lowering the system's degraded exergy. Consequently, the second system will incur greater exergy destruction due to its increased equipment of double-effect absorption chillers compared to the first system.

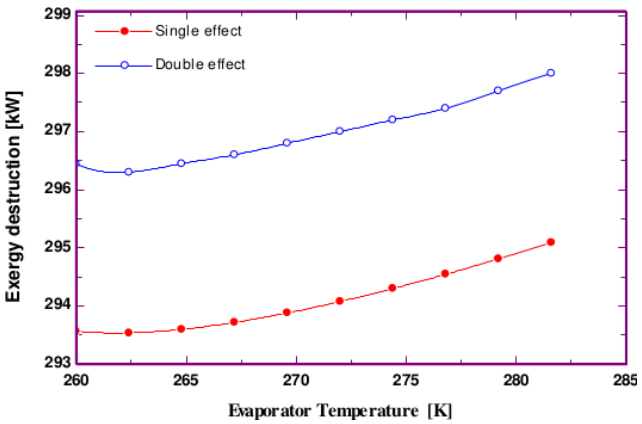


**Fig. 9. Effect of evaporator temperature on exergy destruction of the systems.**

Figure 10 illustrates how exergy efficiency and electricity production costs vary with changes in evaporator temperature. as the evaporator temperature rises, the system's cooling production decreases, leading to reduced exergy efficiency. Conversely, the double effect absorption chiller produces more cooling, resulting in higher exergy efficiency for the second system compared to the first. As the evaporator temperature rises, the cost of electricity produced by the system also increases due to the need for larger equipment to provide cooling, resulting in a higher overall system cost compared to the first system.

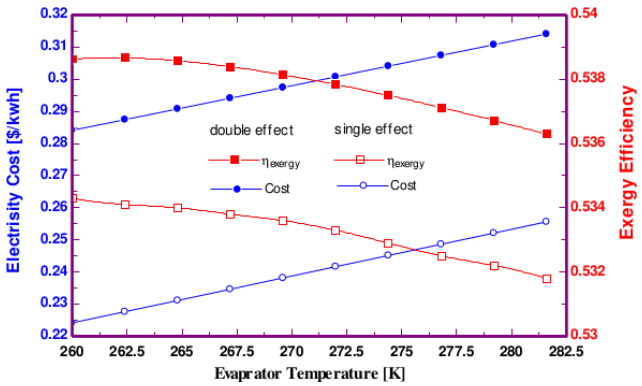


**Fig. 10. Effect of evaporator temperature on exergy efficiency and the price of electricity produced by the systems.**

The analysis below examines the air-to-fuel ratio entering the system. Figures 11 and 12 illustrate how this ratio impacts the cost of electricity produced at a working pressure of approximately 4 bar. The results indicate that as the air-fuel ratio increases, the electricity price decreases. This trend is due to the high temperature and low power output of the fuel cell at low ratios, while at high pressures, increased equipment capacity raises electricity costs. Additionally, a significant decline in energy and exergy efficiency occurs with rising air-to-fuel ratios. The data reveals that the hybrid system demonstrates high production capacity at an air-fuel ratio of 21, where the electricity cost is low. At this ratio and a working pressure of 4 bar, the system can produce about 790 kW, with electricity prices estimated at 0.10 $ and 0.13 $ per kilowatt-hour in the first and second proposed systems, respectively.

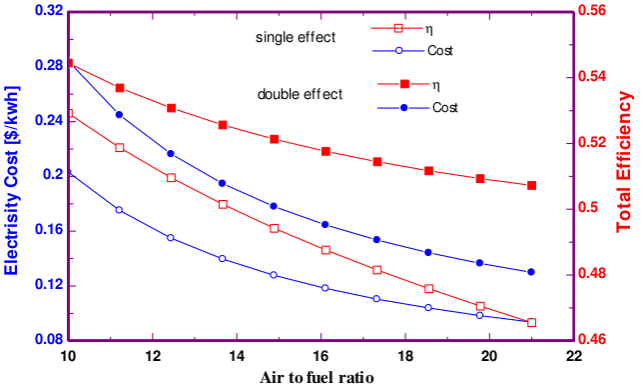


**Fig. 11. Effect of air to fuel ratio on total efficiency and the price of electricity produced by the systems.**

Figure 12 illustrates how the air-fuel ratio affects exergy destruction and exergy efficiency. As the air-fuel ratio increases, exergy destruction rises, leading to a decrease in system efficiency. This increase is more pronounced in the second proposed system compared to the first. Increasing the air input ratio in the system enhances combustion in the chamber, resulting in greater irreversibility and an increase in the system's destroyed exergy.

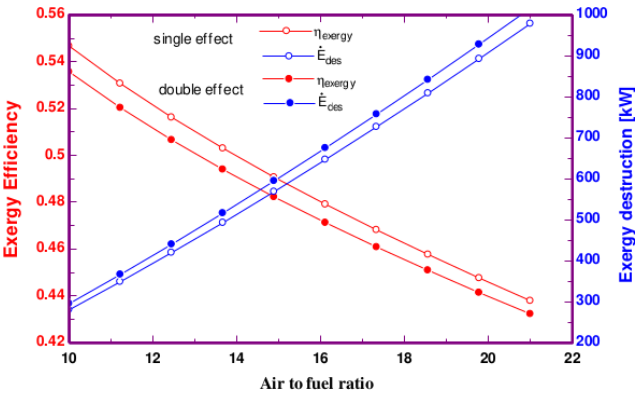


**Fig. 12. Effect of air to fuel ratio on exergy efficiency and exergy destruction of the systems.**

Figure 13 compares the efficiency and price of electricity produced under various conditions. The combined system with an absorption chiller demonstrates higher efficiency due to effective utilization of waste gases. Additionally, the numerous components in this system result in greater electricity production compared to the others.

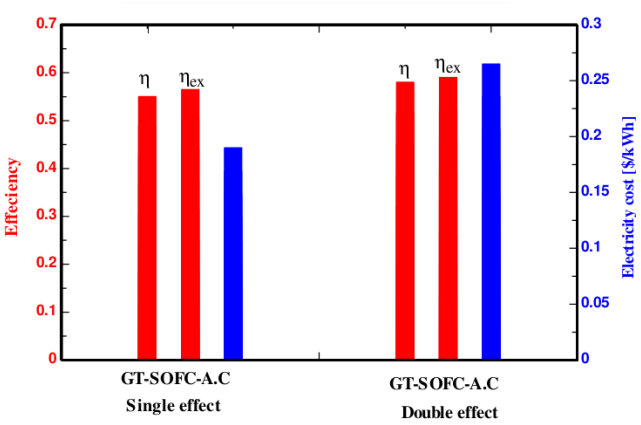


**Fig. 13. Comparing energy and exergy efficiency and the price of electricity produced by the systems.**

## 8 Conclusion

- Increasing the air compressor's working pressure ratio raises the turbine's expansion ratio, reducing exergy destruction, lowering electricity costs, and enhancing system exergy efficiency. Consequently, the second proposed system, due to its equipment, will have a higher electricity price than the first system.
- A higher air-to-fuel ratio boosts the system's power output and lowers electricity costs. At an air-fuel ratio of 21, the maximum power output reaches 790 kilowatts, with the lowest electricity price at 0.14 $ per kilowatt hour.
- Results indicate that the lowest electricity price and highest exergy efficiency occur at a compressor pressure ratio of 6, yielding an exergy efficiency of 0.58 and 0.59 and electricity prices of 0.195 $ and 0.26 $ per kilowatt hour for the first and second systems, respectively.
- Increasing the evaporator's input temperature reduces the systems' cooling output, decreases exergy efficiency, and raises electricity production costs.

## Nomenclature

| | |
|---|---|
| $A$ | Heat transfer area ($m^2$) |
| $C$ | cost per exergy unit ($/GJ) |
| $\dot{C}$ | cost rate |
| $C$ | Heat capacity rate (kW/K) |
| $\dot{\mathrm{E}}\mathrm{x}$ | Exergy rate (kW) |
| $h$ | Enthalpy (kJ/kg) |
| $\dot{m}$ | Mass flow rate (kg/s) |
| $P$ | Pressure (bar) |
| $\dot{Q}$ | Heat rate (kW) |
| $r$ | Pressure ratio |
| $s$ | Specific entropy (kJ/kg.K) |
| $T$ | Temperature (K or °C) |
| $W$ | Power (kW) |
| $V$ | voltage (V) |
| | **Subscripts and abbreviations** |
| c | compressor |
| evap | evaporator |
| gen | generator |
| P | Pump |
| T | Turbine |
| Abs | Absorber |
| ARC | absorption refrigeration cycle |
| CD | condensor |
| GT | Gas Turbine |
| HE | Heat Exchanger |
| SOFC | Solid oxide fuel cell |
| TIT | Turbine Inlet Temperature |
| Th. V | Throttling valve |
| Z | investment cost of components ($) |
| $\dot{Z}$ | investment cost rate of components ($/h) |
| | **Greek symbols** |
| $\eta_{\mathrm{Ex}}$ | Exergy efficiency |
| $\eta_{\mathrm{en}}$ | Energy efficiency |
| $\eta_T$ | Turbine efficiency |
| $\eta_C$ | Compressor efficiency |
| $\epsilon$ | Heat exchanger effectiveness |

## References

[1] Kerr T. Combined heat and power: evaluating the benefits of greater global investment. Retrieved from IEA. 2008;1(22).

[2] Chen X, Zhou H, Li W, Yu Z, Gong G, Yan Y, et al. Multi-criteria assessment and optimization study on 5 kW PEMFC based residential CCHP system. Energy conversion and management. 2018;160:384–395.

[3] Yang X, Zhao H, Hou Q. Proposal and thermodynamic performance study of a novel LNG-fueled SOFC-HAT-CCHP system with near-zero CO2 emissions. International Journal of Hydrogen Energy. 2020;45(38):19691–19706.

[4] Hou Q, Zhao H, Yang X. Thermodynamic performance study of the integrated MR-SOFC-CCHP system. Energy. 2018;150:434–450.

[5] Liu Y, Han J, You H. Performance analysis of a CCHP system based on SOFC/GT/CO2 cycle and ORC with LNG cold energy utilization. International Journal of Hydrogen Energy. 2019;44(56):29700–29710.

[6] Marefati M, Mehrpooya M, Mousavi SA. Introducing an integrated SOFC, linear Fresnel solar field, Stirling engine and steam turbine combined cooling, heating and power process. International Journal of Hydrogen Energy. 2019;44(57):30256–30279.

[7] Ebrahimi-Moghadam A, Moghadam AJ, Farzaneh-Gord M, Arabkoohsar A. Performance investigation of a novel hybrid system for simultaneous production of cooling, heating, and electricity. Sustainable Energy Technologies and Assessments. 2021;43:100931.

[8] Peng MYP, Chen C, Peng X, Marefati M. Energy and exergy analysis of a new combined concentrating solar collector, solid oxide fuel cell, and steam turbine CCHP system. Sustainable Energy Technologies and Assessments. 2020;39:100713.

[9] da Silva FS, Matelli JA. Exergoeconomic analysis and determination of power cost in MCFC–steam turbine combined cycle. International Journal of Hydrogen Energy. 2019;44(33):18293–18307.

[10] Hosseini SS, Mehrpooya M, Alsagri AS, Alrobaian AA. Introducing, evaluation and exergetic performance assessment of a novel hybrid system composed of MCFC, methanol synthesis process, and a combined power cycle. Energy Conversion and Management. 2019;197:111878.

[11] Zeng R, Guo B, Zhang X, Li H, Zhang G. Study on thermodynamic performance of SOFC-CCHP system integrating ORC and double-effect ARC. Energy Conversion and Management. 2021;242:114326.

[12] Zhong L, Yao E, Zou H, Xi G. Thermo-economic-environmental analysis of an innovative combined cooling and power system integrating Solid Oxide Fuel Cell, Supercritical CO2 cycle, and ejector refrigeration cycle. Sustainable Energy Technologies and Assessments. 2021;47:101517.

[13] Behzadi A, Habibollahzade A, Zare V, Ashjaee M. Multi-objective optimization of a hybrid biomass-based SOFC/GT/double effect absorption chiller/RO desalination system with CO2 recycle. Energy conversion and management. 2019;181:302–318.

[14] Zheng N, Duan L, Wang X, Lu Z, Zhang H. Thermodynamic performance analysis of a novel PEMEC-SOFC-based poly-generation system integrated mechanical compression and thermal energy storage. Energy Conversion and Management. 2022;265:115770.

[15] Wang Q, Duan L, Lu Z, Zheng N. Thermodynamic performance comparison of SOFC-MGT-CCHP systems coupled with two different solar

methane steam reforming processes. International Journal of Hydrogen Energy. 2023;48(71):27473–27491.

[16] Zheng N, Zhang H, Duan L, Wang Q. Comprehensive sustainability assessment of a novel solar-driven PEMEC-SOFC-based combined cooling, heating, power, and storage (CCHPS) system based on life cycle method. Energy. 2023;265:126343.

[17] Yang S, Peng S, Xiao Z, Liu Z, Deng C, Du W, et al. Energetic and exergetic analysis of a biomass-fueled CCHP system integrated with proton exchange membrane fuel cell. International Journal of Hydrogen Energy. 2023;48(36):13603–13616.

[18] Ghorbani S, Deymi-Dashtebayaz M, Dadpour D, Delpisheh M. Parametric study and optimization of a novel geothermal-driven combined cooling, heating, and power (CCHP) system. Energy. 2023;263:126143.

[19] Zhang X, Liu W, Pan J, Zhao B, Yi Z, He X, et al. Comprehensive performance assessment of a novel biomass-based CCHP system integrated with SOFC and HT-PEMFC. Energy. 2024;295:131112.

[20] Jia J, Paul MC. Thermodynamic and economic evaluation of a CCHP system with biomass gasifier, Stirling engine, internal combustion engine and absorption chiller. Energy Conversion and Management. 2024;299:117803.

[21] Huang Z, You H, Chen D, Hu B, Liu C, Xiao Y, et al. Thermodynamic, economic, and environmental analyses and multi-objective optimization of a CCHP system based on solid oxide fuel cell and gas turbine hybrid power cycle. Fuel. 2024;368:131649.

[22] Huang S, Duan L, Wang Q, Huang L, Zhang H. Thermodynamic analysis of a CCHP system with hydrogen production process by methane reforming enhanced by solar-assisted chemical looping adsorption. Applied Thermal Engineering. 2024;248:123137.

[23] Wang L, Bo G, Gao R, Ayadi M, Chammam W, Ooi JB, et al. Thermoeconomic assessment of an innovative combined cooling, heating, and power system based on biomass combustion, TCO2 cycle, absorption chiller, and desalination. Process Safety and Environmental Protection. 2024;184:151–169.

[24] Gomri R. Second law comparison of single effect and double effect vapour absorption refrigeration systems. Energy Conversion and Management. 2009;50(5):1279–1287.

[25] Haseli Y, Dincer I, Naterer GF. Thermodynamic modeling of a gas turbine cycle combined with a solid oxide fuel cell. International Journal of hydrogen energy. 2008;33(20):5811–5822.

[26] Haseli Y, Dincer I, Naterer G. Thermodynamic analysis of a combined gas turbine power system with a solid oxide fuel cell through exergy. Thermochimica Acta. 2008;480(1-2):1–9.

[27] Zare V. A comparative thermodynamic analysis of two tri-generation systems utilizing low-grade geothermal energy. Energy conversion and management. 2016;118:264–274.

[28] Yuksel YE, Ozturk M, Dincer I. Energy and exergy analyses of an integrated system using waste material gasification for hydrogen production and liquefaction. Energy Conversion and Management. 2019;185:718–729.

[29] Anvari S, Khalilarya S, Zare V. Exergoeconomic and environmental analysis of a novel configuration of solar-biomass hybrid power generation system. Energy. 2018;165:776–789.

[30] Chan S, Ho H, Tian Y. Modelling of simple hybrid solid oxide fuel cell and gas turbine power plant. Journal of power sources. 2002;109(1):111–120.

[31] Haseli Y, Dincer I, Naterer GF. Thermodynamic modeling of a gas turbine cycle combined with a solid oxide fuel cell. International Journal of hydrogen energy. 2008;33(20):5811–5822.